Differential Integrin Expression Regulates Cell Sensing of the Matrix Nanoscale Geometry

Stefania Di Cio[1,2], Thea M. L. Boggild[3], John Connelly[1,4], Duncan S. Sutherland[3] and Julien E. Gautrot[1,2]*

[1] Institute of Bioengineering and [2] School of Engineering and Materials Science, Queen Mary, University of London, Mile End Road, London, E1 4NS, UK.

[3] Barts and the London School of Medicine and Dentistry, Queen Mary, University of London, 4 Newark Street, London, E1 2AT, UK.

[4] Interdisciplinary Nanoscience Center (iNANO), Aarhus University, Denmark.

* To whom correspondence should be addressed E-mail: j.gautrot@qmul.ac.uk.

Abstract

The nanoscale geometry and topography of the extra-cellular matrix (ECM) is an important parameter controlling cell adhesion and phenotype. Similarly, integrin expression and the geometrical maturation of adhesions they regulate have been correlated with important changes in cell spreading and phenotype. However, how integrin expression controls the nanoscale sensing of the ECM geometry is not clearly understood. Here we develop a new nanopatterning technique, electrospun nanofiber lithography (ENL), which allows the production of a quasi-2D fibrous nanopattern with controlled dimensions (250 – 1000 nm) and densities. ENL relies on electrospun fibres to act as a mask for the controlled growth of protein-resistant polymer brushes. SEM, AFM and immunofluorescence imaging were used to characterise the resulting patterns and the adsorption of the extra-cellular matrix protein fibronectin to the patterned fibres. The control of adhesion formation was studied, as well as the remodelling and deposition of novel matrix. Cell spreading was found to be regulated by the size of fibres, similarly to previous observations made on circular nanopatterns. However, cell shape and polarity were more significantly affected. These changes correlated with important cytoskeleton reorganisation, with a gradual decrease in stress fibre formation as the pattern dimensions decrease. Finally, the differential expression of $\alpha v\beta 3$ and $\alpha 5\beta 1$ integrins in engineered cell lines was found to be an important mediator of cell sensing of the nanoscale geometry of the ECM.

Statement of significance

The novel nanofiber patterns developed in this study, via ENL, mimic the geometry and continuity of natural matrices found in the stroma of tissues, whilst preserving a quasi-2D character (to facilitate imaging and for comparison with other 2D systems such as micropatterned monolayers and circular nanopatches generated by colloidal lithography). These results demonstrate that the nanoscale geometry of the ECM plays an important role in regulating cell adhesion and that this is modulated by integrin expression. This is an important finding as it implies that the knowledge of the biochemical context underlying the integrin-mediated adhesive machinery of specific cell types should allow better design of biomaterials and biointerfaces. Indeed, changes in integrin expression are often associated with the control of cell proliferation and differentiation.

Keywords

Nanopatterning; Polymer brush; Integrin; Focal adhesion.

1. Introduction

Cells are not "free-standing" objects but require to adhere to the *extracellular matrix* (ECM) and to other cells in order to survive, carry out their function and form more complex structures (tissues). It has been shown in the last decades that cells feel and respond to the physical properties of the complex environment constituted by the ECM, contact with neighbouring cells and soluble growth factors and cytokines. Focal adhesion (FA) formation and maturation are important processes via which cells sense and adhere to the ECM and impact on signalling pathways eventually controlling cell phenotype [1, 2]. Such cellular sensing of the adhesive landscape occurs at different length scales, from the microscale, at which cell shape and multi-cellular assemblies are controlled [3-5], to the nanoscale, at which the formation and dynamics of single adhesions are regulated [6-11]. Importantly, underlying these phenomena, the prevention of FA assembly leads to the disruption of the cell cytoskeleton: when cells are forced to adhere on small areas or when adhesion points are too far apart to allow integrin clustering and the interaction of key adapter proteins, cell spreading is impaired and other signalling pathways are disrupted leading, for example, to stem cell differentiation [12, 13].

FAs are initiated and regulated by the binding of integrins to the ECM[14]. This phenomenon is followed by their clustering and the recruitment of other molecules, amongst which vinculin, talin, VASP, zyxin, paxillin, p130 Cas, focal adhesion kinase (FAK) and integrin-linked kinase (ILK) play an important role in determining FA stability and cell phenotype. In addition, the precise positioning of these molecules and 3D organisation of the structure of FAs is important to the stability of FAs formed, their ability to sustain mechanical forces and transmit downstream signals [15, 16]. The dynamics of such processes is regulated by the transmission of forces bidirectionally, inside-out and outside-in: when cells cannot exert adequate grip on their surrounding environment, FAs are destabilised [17]. In turn, the reorganisation of the cell cytoskeleton and formation of stress fibre (contractile actin bundles) are strongly dependent on transmission of intracellular forces. Adapter proteins such as talin and vinculin play an important role in such processes and regulate adhesion size, shape, as well as cell spreading and shape [18-20]. Upon activation of vinculin FAs are generally stabilised, increase in size and, as a result, cell migration decreases. Considering the essential role of integrin clustering to the formation and development of FAs, it is clear that integrin expression itself should have a profound impact on cell adhesion and associated mechanotransduction. Indeed, integrin expression level and the type of heterodimers expressed (e.g. $\alpha5\beta1$ vs $\alpha v\beta3$) was found to impact on cell shape, the architecture of the cytoskeleton, as well as cell motility [21-23]. Such changes are associated with marked changes in signalling via Rho GTPases [22, 24] and, strikingly, the scattering of cell clusters [21]. The shape, number and size of FAs was also found to be strongly correlated with such changes in phenotype [21]. Such effect may be explained by the differential regulation of Rho GTPases Rac and RhoA [22], as well as the differential binding affinity of $\beta1$ and $\beta3$ integrins for soluble fibronectin (and associated impact on fibrillogenesis). These phenomena also correlate with important changes in the dynamics and

nanoscale organisation of α5β1 and αvβ3 integrins [22, 25]. Differential regulation of FA maturation and cell phenotype was also evidenced between different β1 heterodimers (e.g. α5 and α4) [26]. In addition, α5β1 and αvβ3 integrins play important roles in the ability of cells to generate forces, respond to applied mechanical stimulations and associated mechanotransduction [27, 28]. Hence, these studies highlight a direct relationship between integrin expression, the regulation of the shape and size of adhesions and the sensing of physical properties of the ECM.

The sensing of the ECM is thus of particular importance to the regulation of cell phenotype. To investigate the role of different microenvironmental cues, engineered biointerfaces presenting controlled chemistry, topography and mechanical properties have been developed. In particular, the modification of surfaces to create micro- to nano-scale features has been exploited to regulate FA maturation and cell phenotype. Techniques to modify the surface range from bottom-up to top- down approaches. Self- assembly methods have allowed the formation of nanofeatures with controlled spatial distributions [6]. Replication methods such as photolithography and soft lithography are also widely used to reproduce features with the use of a mask or stamp. In the latter, a patterned elastomer is used to print molecules on a surface. Micro contact printing (μCP), which normally uses PDMS, has been widely used to produce protein microarrays for cell-based assays [17, 29, 30]. Combining such μCP with polymer brush growth (after printing of an initiator molecule) allows the generation of particularly stable protein arrays that allow to control cell adhesion over long periods of culture time (beyond 7 days [29]). However, molecular diffusion during the printing process does not allow high resolution patterning (below 1 μm). Direct writing is another approach used to deliver molecules to a surface for chemical patterning: inkjet printing (IJP) and dip-pen nanolithography (DPN) have been applied to the deposition of protein arrays for cell patterning [31, 32]. While high resolution (especially with DPN) and flexible, direct writing approaches are generally slow and with low throughput.

We previously showed that the size of adhesions (100 nm to 3 μm circular patches) primarily controls the assembly of the cytoskeleton, and that blocking the geometrical maturation of adhesions does not restrict protein recruitment significantly, nor the phosphorylation of proteins recruited to adhesions or the assembly of ECM proteins at adhesion sites [10]. In contrast, we found that adhesion dynamics (rate of diffusion of vinculin to the adhesions) was altered. This may highlight the role of adhesion dynamics, assembly and disassembly, as important stages involved in nanoscale sensing. In this respect, the continuity of the matrix, its geometry and topography are expected to regulate such dynamic processes. How such nanoscale geometrical cues impact on adhesion size and shape as well as cell spreading and shape is not understood. In addition, how the differential expression of integrins impacts on the sensing of nanoscale geometry is not clear.

Here we developed a novel patterning platform, electrospun nanofiber lithography (ENL), allowing the generation of cell-adhesive nanofibrous substrates on large scale suitable for the detailed investigation

of mechanisms underlying cell sensing of the nanoscale geometry of the ECM. This platform is based on the deposition of electrospun fibres with controlled diameters in the range of 150 to 1500 nm, which are then used as masks for the controlled growth of protein- and cell-resistant polymer brushes via surface initiated atom transfer radical polymerisation (Figure 1). The nanofibers generated using this method mimic better the fibrous structure of some natural matrices, but without introducing complex 3D effects (topography and changes in fiber curvature). In addition, these quasi-2D nanofibers allow comparison with other 2D nanopatterns displaying circular patches of controlled diameters, previously studied [10]. This allows to investigate relationships between adhesion size and geometry and cell shape and spreading in a more realistic scenario, including with respect to the continuity of the matrix. Finally, as ENL allows the patterning of thin glass coverslips and does not introduce structures with strong refractive index mismatch, it is compatible with a broad range of high resolution live imaging microscopy techniques. This platform was then used to investigate the influence of adhesion geometry on cell spreading and shape. We make comparisons between cell response to the size of nanopatterns in the case of circular discrete patches and continuous nanofibers with similar range of sizes and pattern density. Finally, we investigate the role of integrin expression on nanoscale sensing of the geometry of the adhesive landscape.

2. Materials and methods

2.1 Chemicals and Materials. Oligo(ethylene glycol methyl ether methacrylate) (OEGMA, Mw 300), CuCl, CuCl2, 2,2'-dipyridyl (bpy), Poly (methyl methacrylate) (PMMA) (average Mw ~ 350,000 and 996,000), triethylamine (≥99%), 2,2'-bipyridyl, copper (I) cloride (CuCl), copper(II) bromide (CuBr2), triton X-100, gelatin, Phallodin –Tetramethylrhodamine B isothiocyanate, PFA (paraformaldehyde), Monoclonal AntiVinculin antibody produced in mouse, Mowiol 4-88, glycerol, DAPI (4,6-diamidino-2-phenylindole), GTA (glutaraldehyde), phosphate buffer (PB) 0.1M, phosphate-buffered saline (PBS, 150 mM) and silicon wafers were purchased from Sigma Aldrich. CHCl3 (chloroform, ≥99%), DMF (N, N-Dimethylformamide, ≥99.8%) and toluene were from VWR. Sodium chloride (NaCl) was from fisher chemical. 3-Trimethoxysilylpropyl 2-Bromo-2methyl-propionate was from Fluoro Chem. Precut wafers (P/Boron<100>, SI-MAT) were purchased from Litcon AB (Sweden). PDDA (Poly(diallyldimethylammonium chloride)), PSS (Poly(sodium-4-styrenesulfonate)) and Octadecylmercaptan were purchased from Sigma. PAX-XL60 (polyaluminium chloride) was purchased from Kemira miljø (Denmark). Polystyrene colloidal particles, sulphate latex diameter 0.1 μm, 0.3 μm, 0.6 μm and 3 μm were purchased from Invitrogen (US). Fibronectin from human plasma (1 mg/ml) was from Millipore. Foetal bovine serum (FBS) and was from PAA. DMEM (500 mL), trypsin, versene (100 mL) Alexa Fluor goat anti-mouse 488 were from Life Technologies. Polyclonal anti-Fibronectin antibody (100 μg) and polyclonal anti-laminin from rabbit were from abcam. Penicillin-Streptomycin (5,000 U/mL) L-Glutamine, Alexa Fluor donkey anti rabbit 594 and goat anti rabbit 488 were from Fisher. Deionised water was obtained using a Synergy system from Millipore.

2.2 Silanization. Silicon wafers were treated for 10 min with air plasma (ZEPTO Plasma Etcher from Diener Electronic Plasma Surface Technologies) and then incubated overnight in a solution of 30 µl of 3-trimethoxysilylpropyl 2-bromo-2methyl-propionate (**1**) and 50 µl of triethylamine dissolved in 40 mL toluene. The substrates were then rinsed with DI water, acetone and ethanol and stored under inert atmosphere until used for further treatment.

2.3 Electrospinning. PMMA was used to produce electrospun nanofibers. The polymer was dissolved in a mixture of chloroform and DMF with ratios 7:3 or 6:4. This proportion was selected to guarantee both conductivity (from DMF) and fast evaporation rate (from chloroform) of the solution during the spinning process. Different PMMA concentrations and molecular weight (M_w of 350,000 and 996,000 g/mol) were used to obtain a set of fibre diameters ranging from 150 to 1500 nm (see Supplementary Table S1). The highest M_w PMMA was used for preparing the lowest concentrated solution: this decreased the formation of beads for fibres generated in this condition. To further prevent bead formation for the lowest and highest viscosity solutions (3%, 3.5% and 10%), the addition of salt (NaCl, 0.1 % w/v) which allows to further increase the conductivity of the solution and improve the stretching of fibres was required. To completely allow PMMA to dissolve, the solutions were kept sealed at 50°C overnight whilst stirring.

The solution was loaded in a syringe and supplied to the system using a Kent Genie syringe pump. The solution flowed through a needle fixed at the top of the system and connected to a high DC power supplier (Glassman EQ high voltage) in order to charge the solution. The fibre collector was a metal plate which was grounded. In order to characterise fibre uniformity and the formation of beads, fibres were collected first on glass slides and observed under an optical microscope. The flow rate and voltage were consequently adjusted until beads stopped forming (typically by lowering the flow rate). Typically, the starting flow rate and voltages were 0.3 mL/h and 23 kV, and their range was within 0.2-0.5 mL/h and 21-25 kV, respectively. Fibres were then deposited on silicon wafers previously silanised with the polymerisation initiator **1**. The density of the mats and fibre dimension were confirmed via SEM prior to the next patterning step.

2.4 Annealing. Deposited fibres were thermally annealed in an oven in order to improve their contact with the underlying substrate. The annealing temperature was adjusted for each fibre diameter in order to preserve the fibre dimensions whilst ensuring a good contact with the underlying substrate (see Supplementary Table S2) while incubation time was kept at 1 hr. Substrates were directly placed in the oven, on a metal tray. The thickest fibres were found to require higher annealing temperature in order to deform and bond with the substrate. Fibre dimensions were characterised post-annealing via SEM.

2.5 Colloidal Lithography. Samples were prepared on precut natively oxidized silicon wafers and coated by 4 nm Ti and 30 nm Au (RF magnetron sputtering (home-made), $2x10^{-3}$ mbar argon pressure, Ti deposition rate 1nm/s (6.45 Watt/cm^2), Au deposition rate 2.2 nm/s (2.5 Watt/cm^2). The gold coated

wafers were cleaned with UV/ozone for 1h prior to use followed by immersing in MQ-water for 1h after UV/ozone treatment to allow for the Au_2O_3 formed to be reduced back to Au^0. Nanostructured samples were fabricated via Sparse Colloidal Lithography[39]. A triple layer of PDDA (2% in MQ), PSS (2 % in MQ) and PAX-XL60 (5 % in MQ) was deposited onto the gold coated substrates followed by colloidal assembly of dispersed monolayers of polystyrene particles (100 nm, 300 nm, 600 nm and 3000 nm) by electrostatic self-assembly. Particles concentrations of 0.2 % in MQ for 0.1-0.3 μm, 0.5% for 0.6 μm and 2% for 3 μm particles and deposition times from 120 s to 12 hours were used. After particle deposition, the samples were carefully rinsed, transferred without dewetting to a pressure chamber with MQ-water in which they were heated to 120˚C (140˚C for 3 μm particles). 1nm Ti and 11nm SiO_2 was evaporation coated onto the sample (3kW Multiple Crucible Linear e-Gun, Port Townsend, US. Ti deposition rate 0.5-1Å/s, SiO_2 deposition rate 1-10Å/s). The particles were removed by tape stripping and sonication in ethanol and MQ-water.

Pre-cut nanopatterned substrates (6*6 mm) were placed in a 48-well plate and treated with air plasma for 10 min (Zepto Plasma Etcher from Diener Electronic Plasma Surface Technology) before incubation with an ethanolic solution of octylthiol (Sigma, 5 mM) overnight. The resulting substrates were then washed twice with 70% ethanol and left to sterilise in 70% ethanol for 5 min before washing twice with phosphate buffer saline (PBS, Sigma). The substrates were incubated in a solution of poly(L-lysine)-g-poly(ethylene glycol) PLL(20)-g[3.5]-PEG(2) (Surface Solutions, Switzerland, 25 mg/mL) in (HEPES, 10 mM, pH 7.4, Gibco) for 45 min, then washed with PBS twice.

2.6 Polymer brush growth. Poly oligo(ethylene glycol methyl ether methacrylate) (POEGMA) brushes were used as anti-fouling coating to prevent protein and cell adhesion and to define the background between fibres. POEGMA brushes were grown in between electrospun and annealed PMMA fibres via atom transfer radical polymerization (ATRP) on the target surface pre-functionalized with the silane initiator **1**. The brush thickness was controlled via the polymerization time and monitored via ellipsometry using homogenous silicon substrates functionalised with initiator **1**. The polymerization was carried out under inert gas (typically nitrogen) to avoid the oxidation of the metal catalyst used in the ATRP process. A round-bottom flask containing the monomer/catalyst solution was prepared, containing the monomer (OEGMA, average M_n 300, 12.6 g), the ligand 2,2'-bipyridyl (≥ 99%, 320 mg) and the deactivation catalyst copper(II) bromide ($CuBr_2$, 18 mg) into a mixture of de-ionized water and ethanol (4:1, total volume of 30 mL). The flask was sealed with inert gas inlet and stirred to allow the dissolution of reagents whilst bubbling with inert gas (nitrogen) to remove oxygen from the flask and solution, for 45 min. Copper (I) chloride (CuCl, 82 mg) was quickly added to the solution which was subsequently stirred whilst bubbling with nitrogen for another 15 minutes. The solution was then transferred using a syringe to sealed vials containing the samples (previously degassed and left under inert gas). During the polymerization samples were kept under nitrogen. The polymerisation time was selected depending on the height of the polymer brush required. For 30 nm brushes, polymerization was

carried out for 30 min. Water was then quickly added to the system to stop polymerization and samples were washed with plenty of water to remove any catalyst, then ethanol and dried. The PMMA fibrous masks were then removed from the substrates in Chloroform for 10 min and samples were finally rinsed with water and ethanol and dried. The density of the patterns and fibre dimension were confirmed via SEM.

2.7 Fibronectin deposition. After fibre removal samples were functionalised with fibronectin (FN), which selectively deposited in the gaps left between POEGMA brush coated areas after fibre removal. Samples were incubated for 45 min in a FN solution (10 μg/mL in PBS) at room temperature, then washed with PBS first by diluting twice and then completely replacing the buffer twice more. Cell seeding or immunostaining was carried out directly after this.

2.8 Cell culture and seeding. HaCaT and GE cells were cultured in DMEM supplemented with 10% FBS, glutamine and antibiotics. GE β1-deficient epithelial cells (GE) and GE cells in which α5β1 and αvβ3 integrins are stably expressed (GEβ1 and GEβ3, respectively, obtained by retroviral expression[33][3]) have been previously described (expression levels of α5β1 and αvβ3 integrins are reported in previously published work). Cells were cultured to confluency (about 80% density) and were detached using trypsin/versene (1:9) and reseeded on the samples in a 48 well plate at a density of 7,500 cells/well (1mL/well) in DMEM medium. Cells were then allowed to adhere for 24 hrs and then fixed.

2.9 Immunostaining. After 24 h incubation cells were fixed with 4% paraformaldehyde (in PBS) for 10 min, permeabilized with 0.2% Triton X-100 (in PBS) for 5 min and blocked with a solution of 10% FBS and 0.25% gelatin for 1 h at room temperature. Phalloidin (1:500) was added at this stage too. Samples were then incubated with the primary antibody (anti-vinculin, 1:200) for 1 hr at room temperature, washed and incubated with the conjugated secondary antibody (1:1000; Alexafluor 488) and DAPI (1:1000) for 1 h at room temperature and washed again before being mounted on glass slides with Mowiol solutions.

To check the quality of FN deposition, fibronectin was immunostained. After deposition, samples were blocked for 1 h, then incubated with the fibronectin antibody (anti-fibronectin, 1:200), washed, incubated with the secondary antibody (1:1000; Alexafluor 488 anti-rabbit) for 1 h and finally washed again. All steps were carried out at room temperature. Double staining of fibronectin and vinculin was also carried out. Samples were incubated for 1h at room temperature with primary antibodies (rabbit-α-fibronectin and mouse-α-vinculin mouse) first and then washed and incubated in secondary antibody (in this case using Alexafluor 594 for fibronectin) solutions in blocking buffer (as above) for 1h. For laminin-332 and fibronectin staining, samples were treated first with a 1:1 mixture of FN and labelled BSA (Albumin, Tetramethylrhodamine isothiocyanate bovine, Sigma 10μ/mL) and after cell seeding

they were incubated with primary antibody (anti-laminin, 1:200) and secondary antibody (Alexafluor 488-conjugated, 1:1000).

In order to assess integrin expression in the different cell line (GE, GE β1 and GE β3) double staining of fibronectin/ labelled BSA (as previously described) and either αv (Anti-Integrin alpha V antibody [EPR16800], Abcam) or β1 (Anti-Integrin beta 1 antibody [P5D2], Abcam) integrin monomer was performed.

2.10 Characterization

2.10.1 Ellipsometry. Ellipsometry was used to quantify the thickness of polymer brushes after polymerization on a reference homogenous (no fibre) silicon substrate functionalised with silane **1**. The dry polymer thickness (h_d) was measured using an α-SE® spectroscopic ellipsometer (J. A. Woollam) at an incident angle of 70°. A silicon substrate/Cauchy film model was used and fitted between 400 nm and 900 nm.

2.10.2 SEM. Samples were characterized via scanning electron microscopy (Inspect F from FEI) after each step to check fibre morphology. Fibre diameter was assessed after electrospinning, annealing and polymer brush growth. Fibres were coated with Gold (SC7620 Mini Sputter Coater, Quorum Technologies), 60 sec coating and 20mA process current, whilst this step is not required to image patterns after their removal. A voltage of 20 kV, a spot size of 3.5 and an aperture of 30 μm were used. SEM images were used to assess the pattern density (area were the ECM protein is deposited) and the gap area between the fibres at different fibre sizes using ImageJ. The SEM images are first transformed in black and white images and then the area of the black object (the fibres if density is needed or the area between the fibres when assessing the gaps) is calculated. SEM was also used to investigate cell morphology after adhesion to the patterns. Cells were fixed after 24 h adhesion with 2.5% glutaraldehyde in PB for 2 h at room temperature. Samples were then washed 3 times with PBS 0.1M and dehydrated with a series of ethanol washings increasing the ethanol content from 20% to 100%, each wash repeated twice for 5 minutes. Critical Point Drying was then performed (EMS 850 Critical Point Dryer).

2.10.3 AFM. Atomic force microscopy (AFM- NT-MTD, NTEGRA) was carried out on the patterned samples before and after fibronectin to check the depth of the pattern and the roughness. Semicontact mode was used and the row pictures were corrected with a first order function by the software (Nova). Non-contact NSG01 cantilevers from NT-MDT were used (force constant 1,45-15,1 N/m and resonant frequency 87-230 kHz).

2.11 Immuno-fluorescence microscopy and data analysis. Fluorescence microscopy images to quantify cell spreading (after phalloidin staining), cell density (after nuclear staining with DAPI) and fibronectin deposition (after immunostaining as described above) were acquired with a Leica DMI 4000B

epifluorescence microscope (EL6000 lamp, 20x0.7 NA lens, 63x1.40 Oil lens). Fluorescence microscopy images for vinculin staining were obtained with a Leica TCS SP2 confocal and multiphoton microscope (X-CITE 120 LED lamp, 63X1.4 Oil lens). To quantify cell area, 50-150 cells were analysed and experiments were carried in triplicates at least. Images were analysed with ImageJ, calculating the area of cells after thresholding. For cell density, Dapi staining images thresholding and watershed were used to identify individual nuclei. Profiles for fibronectin stainings were obtained from the corresponding images of immunostained samples, using ImgeJ.

2.12 Statistical analysis. Statistical analysis was carried out using Origin 8 and one-way ANOVA with Tukey test for posthoc analysis. Significance was determined by * $P < 0.05$, ** $P < 0.01$, *** $P < 0.001$. A full summary of statistical analysis is provided below (Supplementary Tables S3-12). In figure captions, "n" means the number of independent replicates of the experiment presented.

3. Results and discussion

3.1 Development of electrospun nanofiber lithography (ENL). In order to pattern 2D-nanofibers on relatively large areas and throughput, allowing comprehensive biological studies, we developed a nano-fabrication technique based on the deposition of sparse mats of electrospun fibres (Figure 1). These mats are used as masks to control the growth of protein and cell resistant polymer brushes from exposed areas. After removal of the fibres, the remaining brushes define a quasi-2D fibrous pattern onto which ECM molecules such as fibronectin can be adsorbed. Therefore this platform is relatively inexpensive, can be scaled up to generate high numbers of substrates in parallel (typically 5-10 microscopy slides can be generated in one batch and cut in smaller samples for seeding in multi-well plates) and compatible with high resolution microscopy, including live TIRF and laser-scanning confocal imaging.

PMMA nanofibers were generated via electrospinning with diameters in the range of 130 ± 10 to 1400 ± 130 nm and deposited onto substrates functionalised with an ATRP initiator. The dimensions of nanofibers was controlled via the molecular weight of the PMMA used, its concentration (in chloroform/DMF solutions) and the presence of an electrolyte (NaCl, see Figure 2B and C and Supplementary Figure S1). The driving voltage and feed solution flow rate were adjusted to suppress the occurrence of beading. This is in good agreement with previous reports that demonstrated the control of Polyethersulfone (PES) [34] and PMMA [35] nanofibers ranging from few hundreds nanometres to microns based on the molecular weight and concentration of materials deposited. In order to improve the contact between fibres and the underlying substrates, an annealing step was carried out prior to brush growth. This had a modest impact on the diameter of nanofibers, as determined by SEM (see Figure 2A and Supplementary Figure S2).

The background of the patterns was passivated next. This was carried out via the growth of a protein and cell resistant polymer brushes based on oligo(ethylene glycol methacrylate) repeat units (POEGMA). Such polymer brushes display excellent protein resistance, due to their hydrophilicity and high packing density and have proved particularly robust for the design of micropatterned cell arrays, even after long incubation times and at high cell densities [5, 29, 30]. POEGMA brushes were grown via surface initiated atom transfer radical polymerisation, which allows a relatively precise control of the thickness of the polymer coatings generated. We targeted a thickness of 30 nm, based on the excellent protein resistance performance of POEGMA for such brush height [29]. After removal of fibres, we found that the height of the brush patterns left, defining the remaining fibrous patterns, was 30 ± 2 nm high, comparable to the thickness predicted and that of homogenous brushes grown in identical conditions and evaluated by ellipsometry (Figure 2A, C and Supplementary Figure S3). The contour profile of the resulting pattern is sharp (90 nm/μm, from AFM profiles) and the width of the resulting fibres closely matches that of the corresponding annealed fibres (Supplementary Figure S2), confirming the efficiency of the fibrous masks to control the localisation of the brush patterns generated via ENL. In addition, we were able to directly image the resulting patterns using SEM, due to the difference in electron density between the exposed silicon substrate and the insulating brush coating. This allowed us to confirm the size of the fibres generated but also their density. We found that large fibres (e.g. 800 nm and 1 μm) displayed a poorer control of the distance between fibres and their density (especially when high densities are desired, Supplementary Figure S4), presumably due to the difficulty of fully annealing the rigid fibres generated with these dimensions.

3.2 Control of protein adsorption and cell adhesion. To enable integrin-mediated cell adhesion, fibronectin was deposited on the patterns (Figure 3A and Supplementary Figure S5). Fluorescence imaging confirmed that fibronectin selectively adsorbed to areas unprotected by POEGMA brushes and formed fibrous fibronectin patterns with controlled dimensions. The intensity profile across fibres within the resulting patterns, with sharp peaks associated with fibronectin fibres (Figure 3A), confirmed the specificity of the protein adsorption and the quality of the resulting patterns. This is in good agreement with results obtained for micro-patterned POEGMA brushes[29], indicating that the initiator layer deposited in the first step of the ENL process remained intact during electrospinning and annealing steps and enabled dense brushes to be generated, with high protein resistance. This also indicates that fibronectin adsorbs well on the exposed fibres to provide a high contrast between fibres and the background. In addition, we examined whether the hydrophobic initiator layer exposed within nanofibers led to the formation of protein clusters and associated changes in nanoscale topography, as was observed during the adsorption of fibronectin to hydrophobic polymers [36, 37]. Measurements of surface roughness via AFM did not highlight any major change in nanoscale topography, either along fibres themselves or within POEGMA-coated areas (Supplementary Figure S6). This confirms that fibronectin deposited homogenously on the nanofibers.

To investigate the control of cell adhesion using the patterns generated via ENL , HaCaT cells were seeded on nanofibrous substrates with fibre widths ranging from 250 to 1000 nm (specifically, 250, 550, 800 and 1000 nm width). In order to assess whether cell adhesions are controlled by the nanoscale geometry of the fibrous pattern, confocal imaging of vinculin (focal adhesion marker) and fibronectin immunostained substrates was carried out (see Figure 3B and Supplementary Figure S5). Colocalization of the two markers was observed, indicating that the geometry of the fibronectin adhesive patterns was efficiently controlling cell adhesion and the maturation of adhesive complexes. This is in good agreement with previous work on circular nanopatches that showed a good control of adhesion geometry using substrates generated via sparse colloidal lithography [10, 38]. These observations were supported by SEM images of HaCaT cells spreading at the surface of nanofibrous substrates (Figure 3D and Supplementary Figure S7). In these images, cell protrusions can be observed to make links with shapes defined by the fibres (despite the low contrast with which quasi-2D fibrous mats can be observed after gold coating of the substrates). In addition, the distal part of these protrusions was found to extend from fibres and be associated with changes in membrane curvature. This led to more irregular geometry of the cell edge and lamellipodiae, compared to cells spreading on homogenous substrates. Lamellipodiae are structures playing an important role in the sensing of physical properties of the matrix and their dynamics and stability controls the formation of stable focal adhesions [39, 40]. Hence, changes in their geometry and dynamics are likely to have an impact on cell spreading and cell shape. Interestingly, cells seeded on wide fibres (800 nm) displayed an increase in contrast in structures observed at areas of lamellipodiae overlapping with fibres (Figure 3D and Supplementary Figure S7). This was not observed on smaller fibres and may indicate an enrichment in cytoskeletal components associated with the recruitment of adhesion molecules at wide fibres and associated stabilisation of lamellipodiae.

Finally, cells can effectively remodel their microenvironment, via deformation of the matrix [41], its degradation[42] or deposition of new ECM proteins [43]. Hence keratinocytes were found to leave trails of laminin-332 during migration [44] and deposit this protein at the surface of circular nanopatches[10]. Such processes may lead to a complete remodelling of the nanoscale geometry of the adhesive landscape as cells spread at biointerfaces. We examined the extent of such phenomena via the immunostaining of HaCaTs spreading on fibronectin nanofibers, probing for the deposition of laminin-332 (Figure 3C and Supplementary Figure S5D). Confocal microscopy indicated that, after 24 h of spreading at the surface of nanofibrous patterns, cells deposited laminin-332 to nanofibers directly in contact with their basal membrane. In addition, double stained cell-seeded substrates (simultaneously probed for fibronectin and laminin-332) showed that the laminin-rich fibres directly extended from the fibronectin fibres onto which cells spread (note that both primary antibodies were raised in the same species and that stainings appear in the same channel). These results indicate that, although ECM protein deposition occurs at the surface of nanopatterned substrates, this phenomenon remains localised to the fibres themselves and

therefore should not significantly impact the geometry of the adhesive landscape, at least during relatively short-term cell adhesion and culture.

3.3 Impact of nanoscale geometry on cell spreading and shape. The extent of cell spreading at the surface of nanofibrous patterns was investigated next. The impact of fibre dimension and density (ratio of ECM-coated area over the total area of the substrate, in this case 60 ± 5 % for high and 22 ± 8 % for low density pattern) was explored first (see Figure 4A and Supplementary Figure S8). The density of cells found to adhere at the surface of patterns after 24 h was relatively insensitive to the size and density of nanofibers. A slight decrease compared to homogenous substrates was observed, potentially due to the lower overall density of ECM proteins. This effect was more pronounced on the largest fibres, perhaps as a result of increased distances between fibres required to preserve the ECM coated area comparable across the range of fibre dimension (Supplementary Figure S4) and prevented the study of cells on the largest fibres at the lowest density. Cell area was more sensitive to the fibre dimensions at low fibre density (22 ± 8 %), although, at high density (60 ± 5 %), changes in cell spreading were still significantly different on the smallest fibres (250 nm) compared to controlled substrates ($P = 0.0002$). Such impact of fibre density may be a result of some level of fibre fusion at higher fibre densities. In addition, changes in cell spreading were found to occur gradually, rather than be sensitive to a specific dimension or density. This is in good agreement with changes in cell spreading reported for adhesion to circular nanopatches [10], but contrasts with observations made in the case of cells spreading on mixed patterns presenting one large adhesive island surrounded by nanopatches, for which an area-threshold was reported [45].

Cell shape was also strongly affected by nanofibers (Figure 4C, D and 5). Whereas HaCaT cells spread isotropically on homogenous control substrates, cells adhering to nanofibers displayed asymmetric polarized shapes. This resulted in an increase in cell aspect ratio on all fibres and a decrease in circularity down to 550 nm fibres, beyond which circularity increases again as a result of the marked decrease in cell spreading observed for cells adhering to 200 nm fibres. At high fibre densities, in agreement with the weaker changes observed in cell spreading, cell shape was not as significant (cell circularity remained unchanged and cell aspect ratio only rose up to 2.2 ± 0.08 for 550 nm fibres).

The changes in cell spreading and shape were correlated with marked changes in the structure of the cytoskeleton (Figure 5). Whereas peripheral transverse actin bundles were typically observed in cells spreading on homogenous substrates [46], cells displayed thick concave stress fibres when spreading on wide nanofibers (800 nm). As the size of nanofibers decreased to 550 and 250 nm, so did the thickness and length of stress fibres, in agreement with the reduction in cell spreading. The formation of stress fibres with associated stable focal adhesions correlates well with the increase in cell polarity and aspect ratio. As the nanofiber size decreased, despite the formation of relatively large focal adhesions, the assembly of stress fibres seems to be gradually prevented, suggesting that, as for cells

adhering to circular nanopatches [10], the nanoscale geometry of the adhesive landscape regulates cytoskeletal assembly rather than focal adhesion protein recruitment.

Having established that cell spreading and shape are determined by fibre diameter, we investigated whether the shape of focal adhesions could influence cell spreading and shape, comparing cell adhesion experiments on nanofibers and circular nanopatches (Supplementary Figure S9). To this aim, we seeded HaCaT cells on circular nanopatches generated via sparse colloidal lithography (with ECM densities comparable to those of the sparse fibres, 20 % of the overall area) [38, 43]. We found a similar trend in cell spreading, as cell area decreased to 449 ± 33 μm^2 on 300 nm patches (Figure 6A), although the larger cell areas observed on the gold control substrates used to compare nanopatches resulted in a stronger decrease in the relative cell spreading for the smallest nanopatches (0.26 ± 0.03 for 300 nm patches, compared to 0.36 ± 0.03 for 250 nm nanofibers). However, cell shape remained largely unaffected by the size of nanopatches and cells spread relatively homogenously and presented only weak polarisation, compared to their behaviour on nanofibers (Supplementary Figure S10). Hence, in addition to focal adhesion size, the shape of adhesive clusters, as determined by the nanoscale geometry of the adhesive landscape, has an important impact on cell spreading and shape.

3.4 Impact of integrin expression on nanoscale sensing of ECM geometry. The expression of different types of integrins strongly influences the size and shape of focal adhesions and this impacts on cell spreading and shape [24]. We next examined whether differential integrin expression could also act as an important sensing element of the nanoscale geometry of the adhesive landscape. The GE cell line is a β1-defficient epithelioid cell line (established from β1-null mouse embryos after clonal culture and selection) expressing low levels of αv and β3 integrins, whereas the GEβ1 and GEβ3 cell lines express high levels of α5β1 and αvβ3 integrins heterodimers, respectively (see Figure S11) [21, 24]. Such integrin expression strongly influences cell morphology and phenotype (e.g. fibrillogenesis, cohesiveness of colonies mimicking an epithelial-mesenchymal transition). In order to study the impact of integrin expression on cell sensing of the nanoscale environment, we seeded these three cell lines on nanofibrous patterns (Figure 6B-D, 7, 8 and Supplementary Figures S12-S14). We found that, although all three cell types responded to the dimensions of nanofibers, the decrease in cell spreading occurred for wider nanofibers and was stronger in the case of αvβ3 expressing cells, in particular GEβ3 cells. We confirmed that the specific integrins expressed were recruited at the nanofibers (Figure S11). Hence whereas the relative cell spreading of GEβ1 cells remained relatively high on 1000 nm-wide fibres (0.8 ± 0.03), it had already decreased significantly on GE and GEβ3 cells (0.63 ± 0.02 and 0.62 ± 0.03, respectively; P = 0.003 and 0.012, respectively). On the thinnest fibres (250 nm), the relative cell spreading of GEβ3 cells was the lowest (0.25 ± 0.03, compared to 0.42 ± 0.03 and 0.44 ± 0.04 for GE and GEβ1 cells, respectively; P = 0.00001 and 0.0010, respectively). These results contrast with those

previously obtained for GE cells spreading onto circular nanopatches, which had indicated that nanoscale sensing of the pattern geometry was insensitive to integrin expression [10].

Focal adhesions assembled by the three types of GE cells were characterised by confocal microscopy. Consistent with previous reports [24], we found that GEβ1 cells adhering to homogenous substrates displayed few elongated focal adhesions, associated with a more polarised morphology, whereas GE and GEβ3 cells displayed many punctate adhesions, with less polarised morphologies (Figures 7-8 and Supplementary Figures S12-S14). The qualitative changes in morphologies observed as a result of differential integrin expression correlated with changes in shape descriptors measured for the three types of GE cells, with higher aspect ratios and lower circularities measured for GEβ1 cells (Figure 7). All three cell lines, upon adhesion to nanofibers, displayed larger and more elongated adhesions, a phenomenon that was most striking for GE and GEβ3 cells. However, for all three cell types, the size and number of adhesions decreased with the size of nanofibres (Figure 9), especially for GEβ3 cells, confirming the control of cell adhesion geometry through ENL, irrespective of integrin expression. This reduction in size was apparent for the largest adhesions, which displayed reduced populations on smaller nanofibers. However, the populations of the largest adhesions (above 2 μm^2) assembled on all nanofibers was higher than for adhesions formed on homogenous substrates. This may indicate that the restricted nanoscale geometry determined by nanofibers contributes to the merging or stabilisation of adhesions into larger complexes. This is however insufficient to maintain the spreading area observed for cells on control homogenous substrates and indicates that ECM geometry may directly impact on the assembly of other structures than focal adhesions, such as the actin cytoskeleton, to regulate spreading. Overall, the reduction in ECM adhesion size and numbers was associated with a disruption of the structure of the cytoskeleton, with shorter and thinner actin fibres originating from adhesions formed on smaller nanofibers (Supplementary Figures S12-S14).

Our results suggest that, although cell adhesion is correlated with the size of nanofibers, differential expression of integrin heterodimers is an important mediator of the sensing of the nanoscale geometry of the adhesive landscape. Hence, β1-expressing cells are less susceptible to the dimension of nanofibers compared to β3-expressing cells. We hypothesise that the ability of β1-expressing cells to retain a spread morphology on nanofibers may be related to their polarised morphology, even on homogenous substrates. Therefore, spreading on nanofibers does not force β1-expressing cells to adopt an abnormal polarised phenotype, whereas β3-expressing cells are strongly induced to polarise on nanofibers.

4. Conclusion

Overall, our results show that the nanoscale geometry of adhesions is an important regulator of cell spreading and shape. In contrast to circular nanopatches that restrict the geometrical maturation of adhesions via the control of their size, nanofibers allow adhesions to develop along one axis. From this point of view, nanofibrous patterns, although 2D, mimic better the continuity and geometry of natural fibrous matrices, often found for example in the mesenchyme and stroma. The parallels observed between cell spreading on circular and fibrous patterns indicate that the size of adhesions regulates the assembly of the actin cytoskeleton. However, the ability of adhesions to develop along one dimension on nanofibers result in the polarisation of cells that otherwise would adopt symmetric shapes on homogenous substrates. Such sensing of the nanoscale geometry of the adhesive landscape offers strong parallels with the spreading of cells on surfaces regulating the topography of self-assembled fibronectin [47]. Our results also demonstrate that differential expression of integrins modulates sensing of nanoscale geometrical cues. Considering the importance of differential integrin expression to the mechanical sensing of the matrix and response to deformation [27, 28], integrin-specific physical sensing of the microenvironment appears as a general phenomenon. In this respect, developing differential expression of integrins may provide an adaptive advantage for cells able to sense and respond to the physical properties of their micro-environment. This may explain some of the differences typically observed in integrin expression between epithelial and mesenchymal tissues. Our findings highlight the importance of understanding the specific sensing mechanisms of nanoscale physical cues in order to develop appropriate implant texturing designs for promoting the adhesion of specific cell types (and potentially controlling their phenotype). However, the detailed mechanism via which integrin ligation mediates the sensing of nanoscale geometrical cues remain elusive. The reorganisation of the cytoskeleton seems to play an important role in this process, but key steps and parameters controlling this phenomenon are not clearly understood.

Acknowledgment

We thank Prof. Arnoud Sonnenberg for sharing GE cell lines used in this study. Funding from Institute of Bioengineering (Queen Mary, University of London) and from the Engineering and Physical Sciences Research Council (EP/J501360/1) is gratefully acknowledged.

Appendix A. Supplementary data

Supplementary data associated with this article can be found, in the online version, at

Figure 1. Method used for patterning: electrospun fibres are used as a mask to protect areas from polymer brush growth (the non-fouling background), prior to their removal via dissolution in chloroform. Protein adsorption to the resulting unprotected areas is then carried out from solution and generates 2D ECM protein nanofibers that will define the nanoscale geometry of cell adhesions.

Figure 2. A. SEM pictures. Top row: electrospun fibres 200 nm (left) and 1000 nm (right). Middle row: 200 nm fibre before (left) and after (right) annealing at 140˚C. Bottom row: 250 nm (left) and 1000nm (right) fibre pattern after mask removal. Scale bar is 10 μm. B. Fibre dimensions obtained using different PMMA concentration and with or without the use of an electrolyte (with SE). For statistical test: *, $P < 0.05$; **, $P < 0.01$; ***, $P < 0.001$; ****, $P < 0.0001$. C. AFM of 1000, nm fibres pattern with height profile. Scale bar is 2, μm.

Figure 3. A. Images from epifluorescence microscopy: 200 nm (left) 800 nm (right) patterns after fibronectin deposition and immunostaining. The inset shows the corresponding fibronectin intensity profile. Scale bar 50 μm. B. Confocal microscopy images of cells on 600 nm fibres (first image from the left, scale bar 10 μm): vinculin (green) and fibronectin (red). Zooms of the region delimited by dashed box (scale bar 2 μm). C. Confocal images of immunostained samples: laminin on 1000 nm patterns (right) and FN/BSA (1/1, 594nm, red) and laminin (green) on 550 nm patterns (left). Scale bar is 10 μm. D. SEM images of HaCaT cells growing on 300 nm (left) and 800 nm (right) patterns. Scale bar 10 μm.

Figure 4. HaCat cell spreading and relative area change on low (A) and high (B) density pattern with fibres dimensions of 250, 550 and 800 nm. Ctrl is the homogenous control surface. Cell morphology quantified via circularity and aspect ratio on low (C) and high (D) density patterns. Error bars are SE, $n \geq 3$, with n representing the number of experiments. For statistical test: **, $P < 0.01$; ***, $P < 0.001$; ****, $P < 0.0001$.

Figure 5. Confocal images of HaCat cells spreading on different size patterns: vinculin (green) and actin (red) staining of cell spreading on control homogenous surfaces (first column, Ctrl), 800 nm (second column), 550 nm (third column) and 250 nm (last column) patterns (low density). Scale bar is 10 μm.

Figure 6. A. HaCat cell spreading and relative area change on circular patches (see corresponding SEM image at the top and in Supplementary Figure S9). Cell spreading and relative area change of GE11 (B), GE11β1 (C) and GE11β3 (D) on fibrous patterns (see SEM image, scale bars are 10 μm, and schematics of integrin expression at the top) in the boxes. Ctrl is the homogenous control surface. Error bars are SE ($n \geq 6$, with n representing the number of experiments). For statistical test: **, $P < 0.01$; ***, $P < 0.001$; ****, $P < 0.0001$; *****$P < 0.00001$.

Figure 7. GE cell density on different pattern size (A). Shape descriptor (circularity and aspect ratio), for GE (B), GE β1 (C) and GE β3 (D) cells on different pattern sizes. Ctrl is the homogenous control surface. Error bars are SE, $n \geq 4$, with n representing the number of experiments. For statistical test: *, $P < 0.05$; **, $P < 0.01$; ***, $P < 0.001$; ****, $P < 0.0001$.

Figure 8. Confocal images: vinculin (green) and actin (red) staining of cell spreading on control homogenous surfaces (first column, Ctrl), 800 (for HaCat on circular patches)/ 1000 nm (for GE cells) (second column), 500 nm (third column) and 250 nm (last column) patterns (low density). Scale bar 10 μm.

Figure 9. A, B and C: focal adhesion distribution for the GE11, GE11 β1 and GE11 β3 cells (respectively) on the different pattern size. D: total number of FA per cell for each condition. Ctrl is the homogenous control surface. Error bars are SE, $n = 3$, with n representing the number of experiments. For statistical test: *, $P < 0.05$; **, $P < 0.01$; ***, $P < 0.001$; ****, $P < 0.0001$.

Figure 1

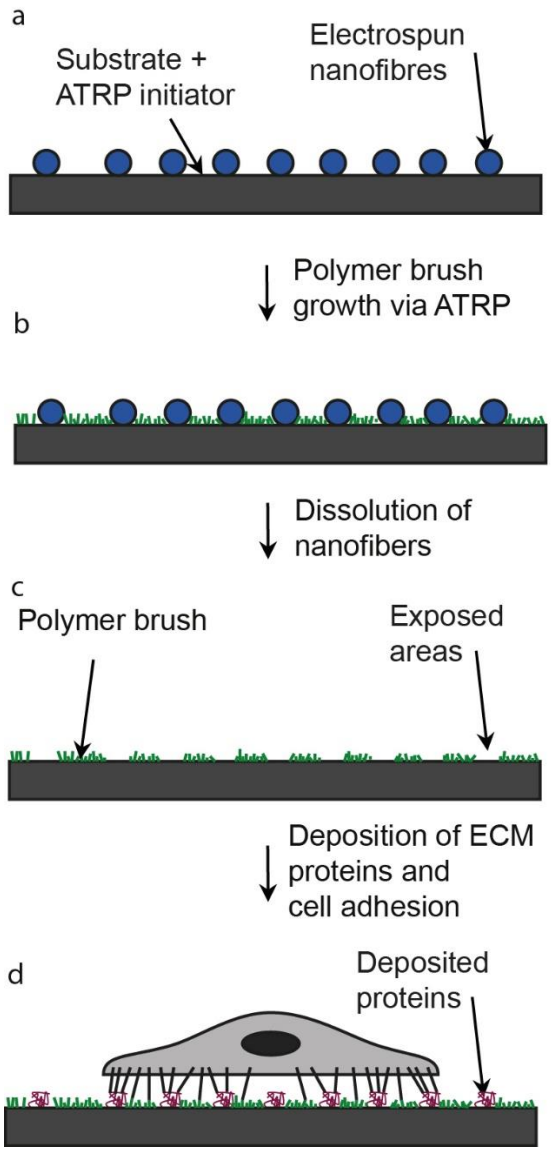
a
Substrate +
ATRP initiator
Electrospun
nanofibres
Polymer brush
growth via ATRP
b
Dissolution of
nanofibers
c
Polymer brush
Exposed
areas
Deposition of ECM
proteins and
cell adhesion
d
Deposited
proteins

Figure 2

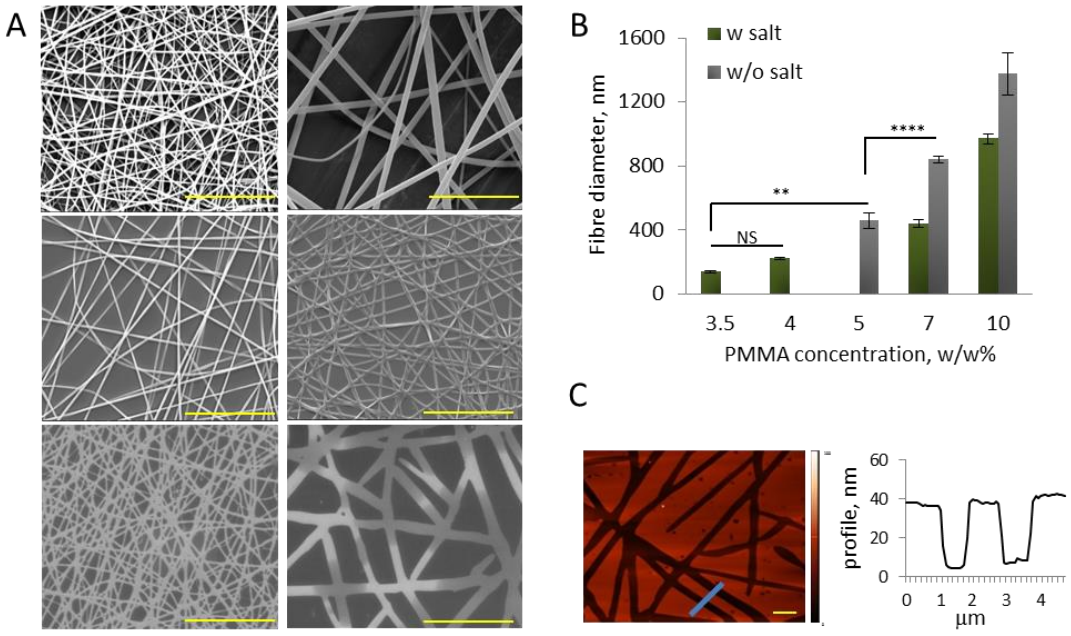
A
B
w salt
w/o salt
1600
1200
800
400
0
Fibre diameter, nm
NS
**
****
3.5
4
5
7
10
PMMA concentration, w/w%
C
60
40
20
0
profile, nm
0
1
2
3
4
µm

Figure 3

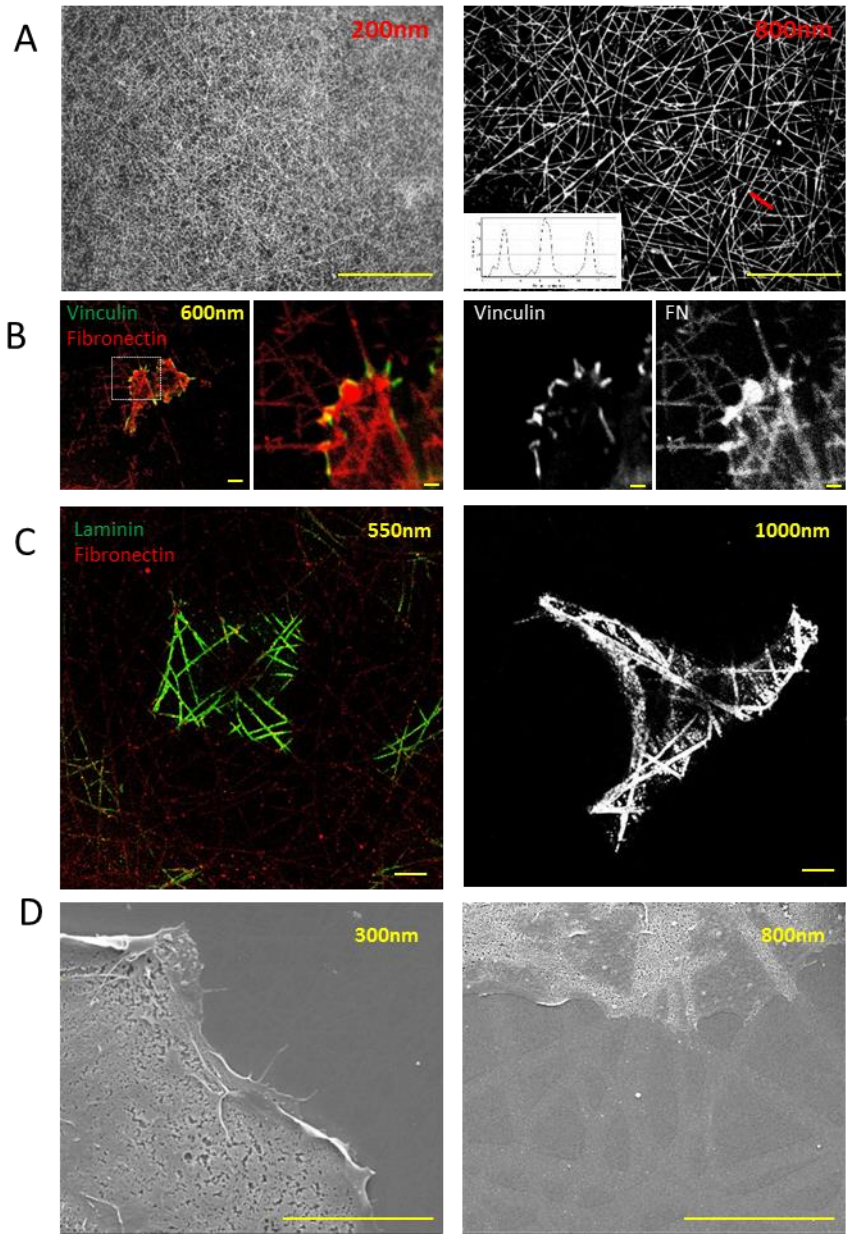
A
200nm
800nm
B
Vinculin
Fibronectin
600nm
Vinculin
FN
C
Laminin
Fibronectin
550nm
1000nm
D
300nm
800nm

Figure 4

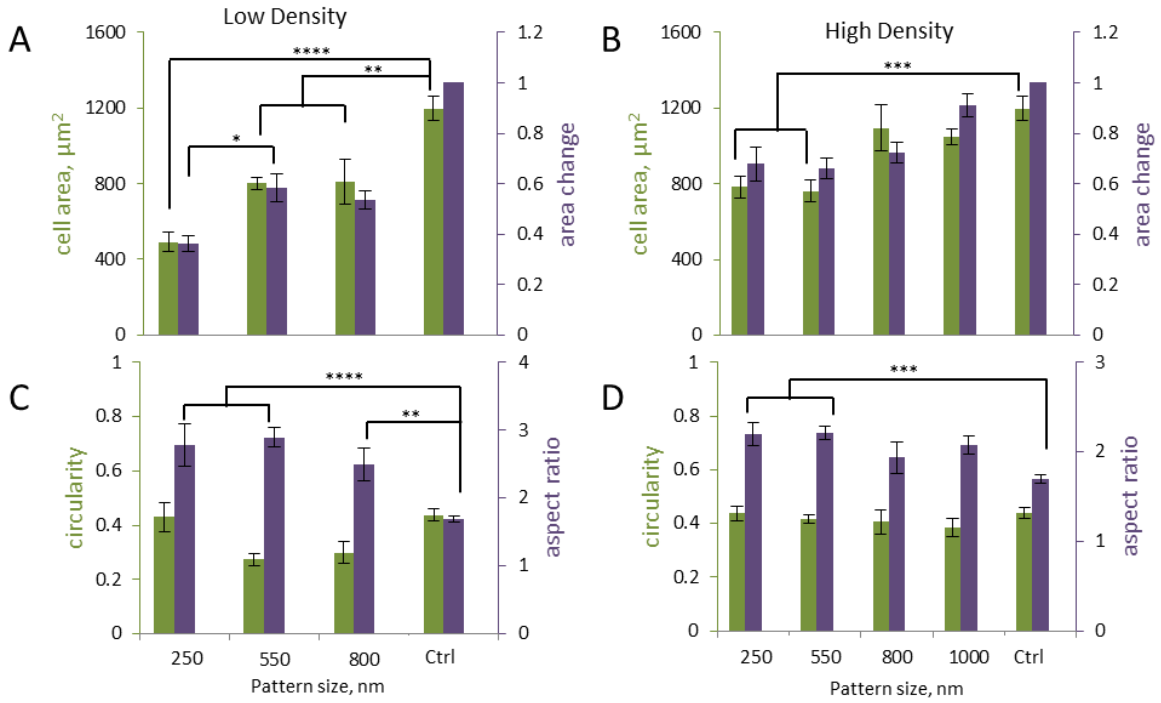
A
Low Density
cell area, µm²
area change
****
**
*
B
High Density
***
C
circularity
aspect ratio
****
**
D
***
250
550
800
1000
Ctrl
Pattern size, nm

Figure 5

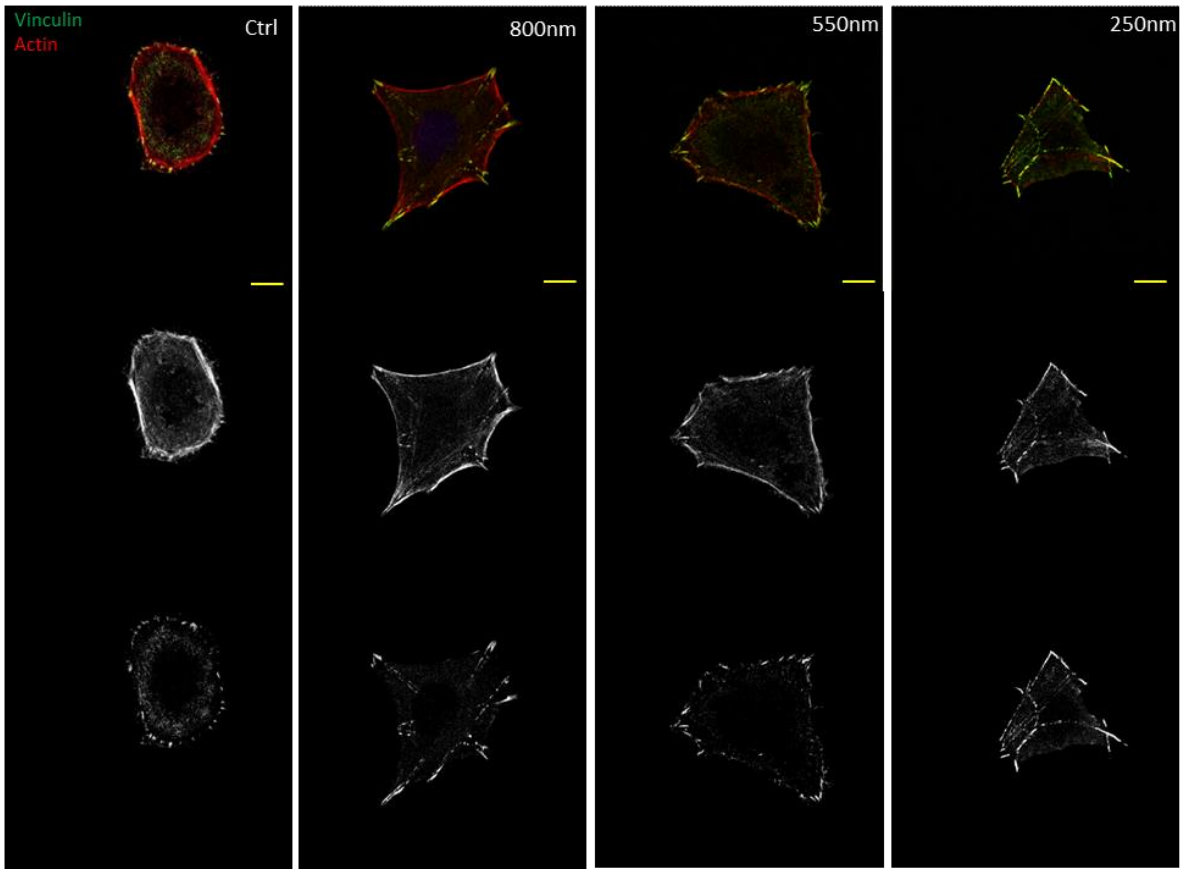

Figure 6

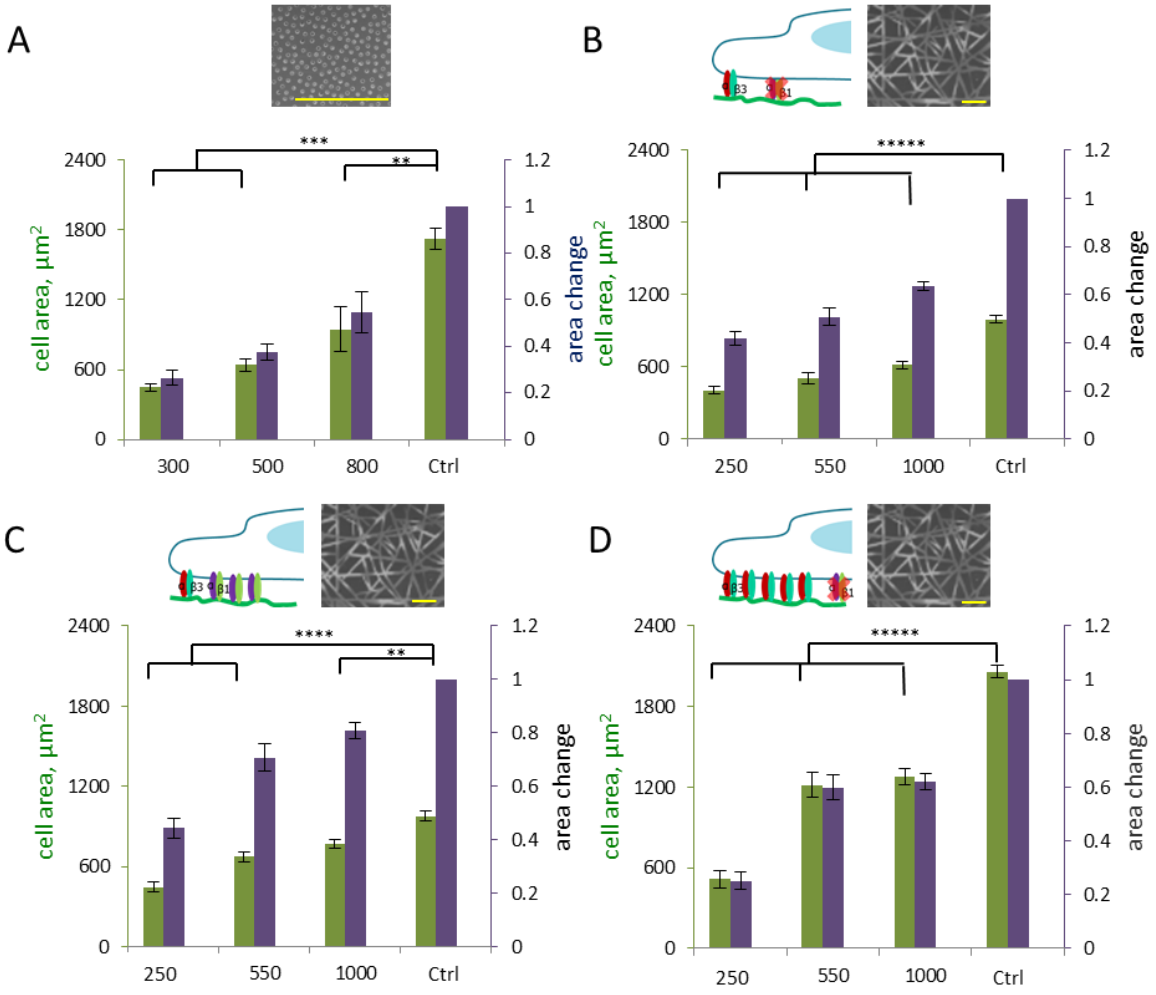
A
B
C
D
cell area, µm²
area change
2400
1800
1200
600
0
1.2
1
0.8
0.6
0.4
0.2
0
300
500
800
Ctrl
250
550
1000
***
**
*****
****

Figure 7

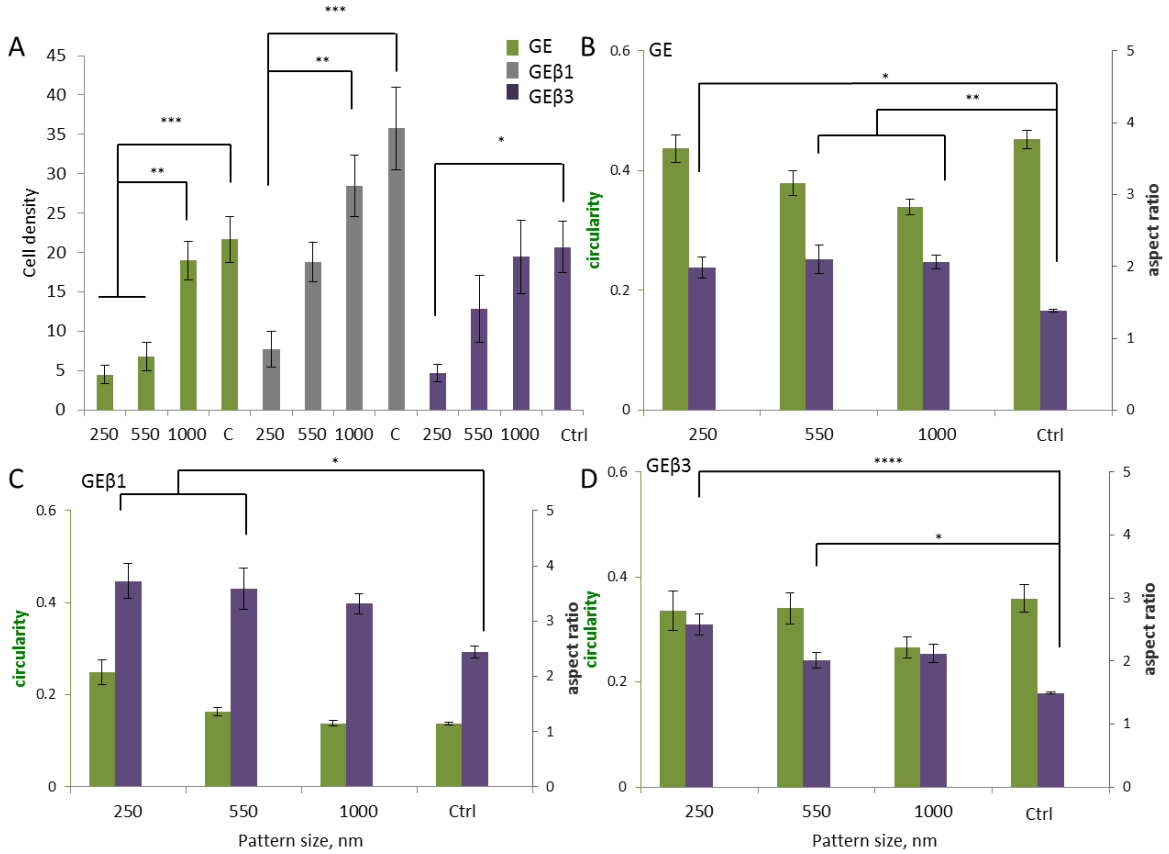
A
GE
GEβ1
GEβ3
Cell density
250 550 1000 C 250 550 1000 C 250 550 1000 Ctrl
B
GE
circularity
aspect ratio
250 550 1000 Ctrl
C
GEβ1
circularity
aspect ratio
250 550 1000 Ctrl
Pattern size, nm
D
GEβ3
circularity
aspect ratio
250 550 1000 Ctrl
Pattern size, nm

Figure 8

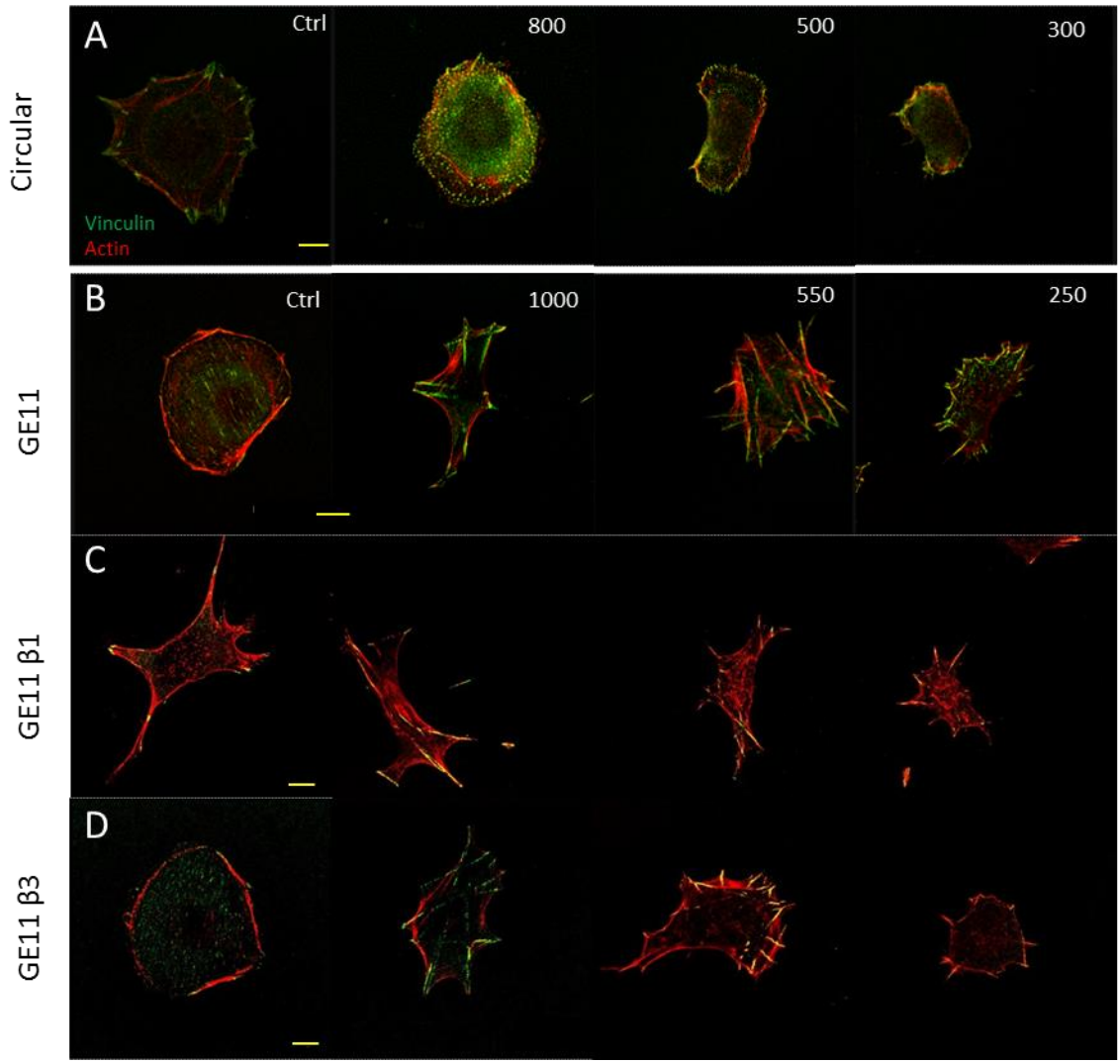
A
Ctrl
800
500
300
Circular
Vinculin
Actin
B
Ctrl
1000
550
250
GE11
C
GE11 β1
D
GE11 β3

Figure 9

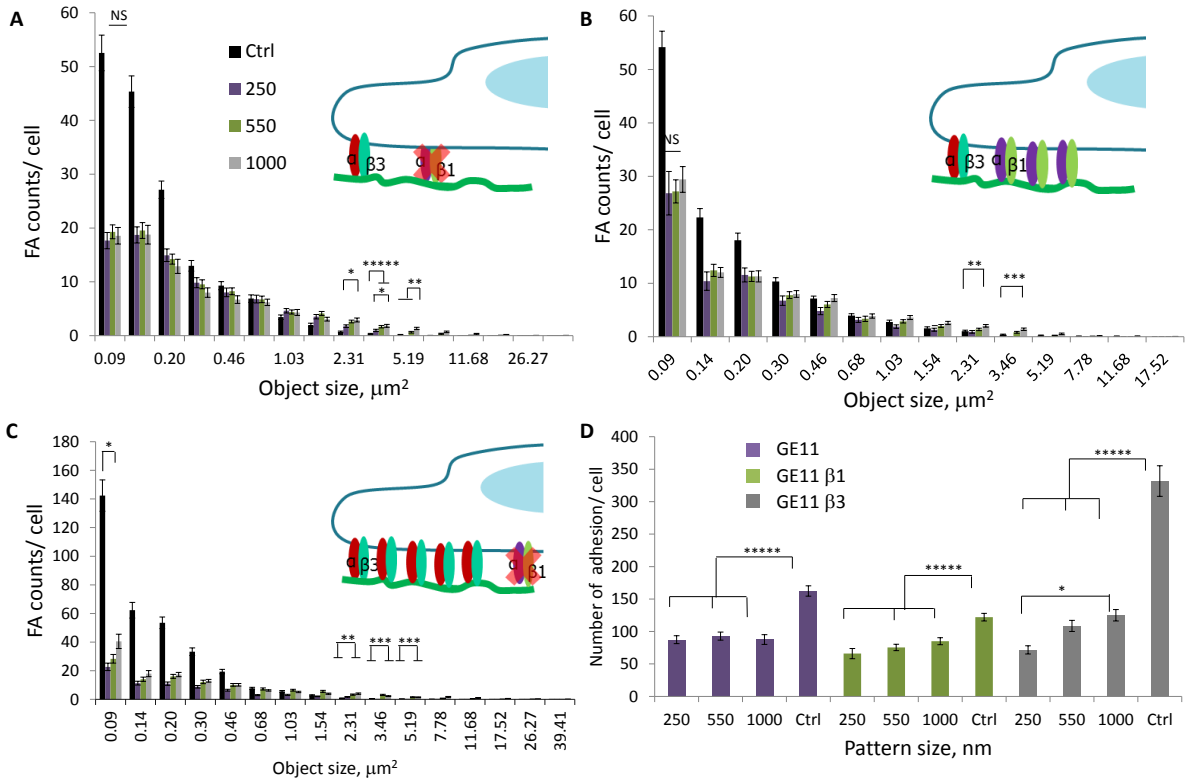
A
NS
Ctrl
250
550
1000
FA counts/ cell
Object size, µm²
B
NS
FA counts/ cell
Object size, µm²
C
FA counts/ cell
Object size, µm²
D
GE11
GE11 β1
GE11 β3
Number of adhesion/ cell
Pattern size, nm

References

[1] Berrier AL, Yamada KM. Cell–matrix adhesion. J Cell Physiol.213 (2007) 565-73.
[2] Parsons JT, Horwitz AR, Schwartz MA. Cell adhesion: integrating cytoskeletal dynamics and cellular tension. Nat Rev Mol Cell Bio. 11 (2010) 633-43.
[3] McBeath R, Pirone DM, Nelson CM, Bhadriraju K, Chen CS. Cell shape, cytoskeletal tension, and RhoA regulate stem cell lineage commitment. Dev Cell 6 (2004) 483-95.
[4] Connelly JT, Gautrot JE, Trappmann B, Tan DW, Donati G, Huck WT, Watt FM. Actin and serum response factor transduce physical cues from the microenvironment to regulate epidermal stem cell fate decisions. Nat Cell Biol 12 (2010) 711-8.
[5] Gautrot JE, Wang C, Liu X, Goldie SJ, Trappmann B, Huck WTS, Watt FM. Mimicking normal tissue architecture and perturbation in cancer with engineered micro-epidermis. Biomaterials 33 (2012) 5221-9.
[6] Huang J, Grater SV, Corbellini F, Rinck S, Bock E, Kemkemer R, Kessler H, Ding J and Spatz JP . Impact of order and disorder in RGD nanopatterns on cell adhesion. Nano Lett 9 (2009) 1111-6.
[7] Schvartzman M, Palma M, Sable J, Abramson J, Hu X, Sheetz MP, Wind SJ. Nanolithographic control of the spatial organization of cellular adhesion receptors at the single-molecule level. Nano Lett 11 (2011) 1306-12.
[8] Cavalcanti-Adam EA, Micoulet A, Blummel J, Auernheimer J, Kessler H, Spatz JP. Lateral spacing of integrin ligands influences cell spreading and focal adhesion assembly. Eur J Cell Biol 85 (2006) 219-24.
[9] Dalby MJ, Gadegaard N, Tare R, Andar A, Riehle MO, Herzyk P, Wilkinson CDW and Oreffo ROC . The control of human mesenchymal cell differentiation using nanoscale symmetry and disorder. Nat Mater 6 (2007) 997-1003.
[10] Gautrot JE, Malmstrom J, Sundh M, Margadant C, Sonnenberg A, Sutherland DS. The nanoscale geometrical maturation of focal adhesions controls stem cell differentiation and mechanotransduction. Nano Lett 14 (2014) 3945-52.
[11] Di Cio S, Gautrot JE. Cell sensing of physical properties at the nanoscale: Mechanisms and control of cell adhesion and phenotype. Acta Biomater 30 (2016) 26-48.
[12] Biggs MJP, Richards RG, Gadegaard N, Wilkinson CDW, Oreffo ROC, Dalby MJ. The use of nanoscale topography to modulate the dynamics of adhesion formation in primary osteoblasts and ERK/MAPK signalling in STRO-1+enriched skeletal stem cells. Biomaterials 30 (2009) 5094-103.
[13] Lee MR, Kwon KW, Jung H, Kim HN, Suh KY, Kim K and Kim K-S. Direct differentiation of human embryonic stem cells into selective neurons on nanoscale ridge/groove pattern arrays. Biomaterials 31 (2010) 4360-6.
[14] Petit V, Thiery JP. Focal adhesions: structure and dynamics. Biol Cell 92 (2000) 477-94.
[15] Kanchanawong P, Shtengel G, Pasapera AM, Ramko EB, Davidson MW, Hess HF, and Waterman CM. Nanoscale architecture of integrin-based cell adhesions. Nature 468 (2010) 580-4.
[16] Case LB, Baird MA, Shtengel G, Campbell SL, Hess HF, Davidson MW, and Waterman CM. Molecular mechanism of vinculin activation and nanoscale spatial organization in focal adhesions. Nat Cell Biol 17 (2015) 880-92.
[17] Gallant ND, Michael KE, Garcia AJ. Cell adhesion strengthening: contributions of adhesive area, integrin binding, and focal adhesion assembly. Mol Biol Cell 16 (2005) 4329-40.
[18] Liu J, Wang Y, Goh WI, Goh H, Baird MA, Ruehland S, Teo S, Bate N, Critchley DR, Davidson MW, and Kanchanawong P . Talin determines the nanoscale architecture of focal adhesions. PNAS 112 (2015) E4864-E73.
[19] Carisey A, Tsang R, Greiner AM, Nijenhuis N, Heath N, Nazgiewicz A, Kemkemer R, Derby B, Spatz J and Ballestrem C . Vinculin regulates the recruitment and release of core focal adhesion proteins in a force-dependent manner. Curr Biol 23 (2013) 271-81.
[20] Humphries JD, Wang P, Streuli C, Geiger B, Humphries MJ, Ballestrem C. Vinculin controls focal adhesion formation by direct interactions with talin and actin. J Cell Biol 179 (2007) 1043-57.

[21] Gimond C, Van Der Flier A, Van Delft S, Brakebusch C, Kuikman I, Collard JG, Fässler R, Sonnenberg A. Induction of cell scattering by expression of β1 integrins in β1-deficient epithelial cells requires activation of members of the rho family of GTPases and downregulation of cadherin and catenin function. J Cell Biol 147 (1999) 1325-40.
[22] Danen EH, van Rheenen J, Franken W, Huveneers S, Sonneveld P, Jalink K, Sonnenberg A. Integrins control motile strategy through a Rho–cofilin pathway. J Cell Biol 169 (2005) 515-26.
[23] Truong H, Danen EH. Integrin switching modulates adhesion dynamics and cell migration. Cell adh migr 3 (2009) 179-81.
[24] Danen EH, Sonneveld P, Brakebusch C, Fässler R, Sonnenberg A. The fibronectin-binding integrins α5β1 and αvβ3 differentially modulate RhoA–GTP loading, organization of cell matrix adhesions, and fibronectin fibrillogenesis. J Cell Biol 159 (2002) 1071-86.
[25] Rossier O, Octeau V, Sibarita JB, Leduc C, Tessier B, Nair D, Gatterdam V, Destaing O, Albigès-Rizo C, Tampé R, Cognet L, Choquet D, Lounis B and Giannone G. Integrins beta1 and beta3 exhibit distinct dynamic nanoscale organizations inside focal adhesions. Nat Cell Biol 14 (2012) 1057-67.
[26] Mostafavi-Pour Z, Askari JA, Parkinson SJ, Parker PJ, Ng TT, Humphries MJ. Integrin-specific signaling pathways controlling focal adhesion formation and cell migration. J Cell Biol 161 (2003) 155-67.
[27] Roca-Cusachs P, Gauthier NC, del Rio A, Sheetz MP. Clustering of α5β1 integrins determines adhesion strength whereas αvβ3 and talin enable mechanotransduction. PNAS 106 (2009) 16245–50.

[28] Balcioglu H. E., Hedde van Hoorn, Dominique M. Donato, Thomas Schmidt, Danen aEHJ. The integrin expression profile modulates orientation and dynamics of force transmission at cell–matrix adhesions. J Cell Sci 128 (2015) 1316-26.
[29] Gautrot JE, Trappmann B, Oceguera-Yanez F, Connelly J, He X, Watt FM, and Huck WTS. Exploiting the superior protein resistance of polymer brushes to control single cell adhesion and polarisation at the micron scale. Biomaterials 31 (2010), 5030-41.
[30] Tan KY, Lin H, Ramstedt M, Watt FM, Huck WT, Gautrot JE. Decoupling geometrical and chemical cues directing epidermal stem cell fate on polymer brush-based cell micro-patterns. Integr Biol 5 (2013), 899-910.
[31] Ginger DS, Zhang H, Mirkin CA. The evolution of dip-pen nanolithography. Angewandte Chemie 43 (2004), 30-45.
[32] Wilson DL, Martin R, Hong S, Cronin-Golomb M, Mirkin CA, Kaplan DL. Surface organization and nanopatterning of collagen by dip-pen nanolithography. PNAS 98 (2001), 13660-4.
[33] Danen EHJ, Sonneveld P, Brakebusch C, Fassler R, Sonnenberg A. The fibronectin-binding integrins $\alpha5\beta1$ and $\alpha v\beta3$ differentially modulate RhoA-GTP loading, organization of cell matrix adhesions, and ifbronectin fibrillogenesis. J Cell Biol 159 (2002), 1071-86.
[34] Christopherson GT, Song H, Mao HQ. The influence of fiber diameter of electrospun substrates on neural stem cell differentiation and proliferation. Biomaterials 30 (2009), 556-64.
[35] Liu Y, Ji Y, Ghosh K, Clark RA, Huang L, Rafailovich MH. Effects of fiber orientation and diameter on the behavior of human dermal fibroblasts on electrospun PMMA scaffolds. J Biomed Mater Res A 90 (2009), 1092-106.
[36] Guerra NB, González-García C, Llopis V, Rodríguez-Hernández JC, Moratal D, Rico P, Salmerón-Sánchez M. Subtle variations in polymer chemistry modulate substrate stiffness and fibronectin activity. Soft Matter 6 (2010), 4748-55.
[37] Bathawab FM, Bennett MAP, Cantini M, Reboud J, Dalby MJ, Salmerón-Sánchez M. Lateral Chain Length in PolyAlkyl Acrylates Determines the Mobility of Fibronectin at the Cell/Material Interface. Langmuir 2015.
[38] Malmstrom J, Christensen B, Jakobsen HP, Lovmand J, Foldbjerg R, Sorensen ES, Sutherland DS. Large area protein patterning reveals nanoscale control of focal adhesion development. Nano Lett 94 (2010), 686-94.

[39] Giannone G, Dubin-Thaler BJ, Döbereiner H-G, Kieffer N, Bresnick AR, Sheetz MP. Periodic lamellipodial contractions correlate with rearward actin waves. Cell 116 (2004), 431-43.
[40] Gardel ML, Sabass B, Ji L, Danuser G, Schwarz US, Waterman CM. Traction stress in focal adhesions correlates biphasically with actin retrograde flow speed. J Cell Biol 183 (2008), 999-1005.
[41] Huebsch N, Arany PR, Mao AS, Shvartsman D, Ali OA, Bencherif SA, Rivera-Feliciano J and Mooney DJ. Harnessing traction-mediated manipulation of the cell/matrix interface to control stem-cell fate. Nat Mater 9 (2010), 518-26.
[42] Khetan S, Guvendiren M, Legant WR, Cohen DM, Chen CS, Burdick JA. Degradation-mediated cellular traction directs stem cell fate in covalently crosslinked three-dimensional hydrogels. Nat Mater 12 (2013), 458-65.
[43] Malmström J, Lovmand J, Kristensen S, Sundh M, Duch M, Sutherland DS. Focal Complex Maturation and Bridging on 200 nm Vitronectin but Not Fibronectin Patches Reveal Different Mechanisms of Focal Adhesion Formation. Nano Lett 11 (2011), 2264–71.
[44] Frank DE, Carter WG. Laminin 5 deposition regulates keratinocyte polarization and persistent migration. J Cell Sci 117 (2004), 1351-63.
[45] Coyer SR, Singh A, Dumbauld DW, Calderwood DA, Craig SW, Delamarche E, García AJ. Nanopatterning reveals an ECM area threshold for focal adhesion assembly and force transmission that is regulated by integrin activation and cytoskeleton tension. J Cell Sci 125 (2012), 5110-23.
[46] Tee YH, Shemesh T, Thiagarajan V, Hariadi RF, Anderson KL, Page C, Volkmann N, Hanein D, Sivaramakrishnan S, Kozlov MM and Bershadsky AD . Cellular chirality arising from the self-organization of the actin cytoskeleton. Nat Cell Biol 17 (2015), 445-57.
[47] Vanterpool FA, Cantini M, Seib FP, Salmeron-Sanchez M. A material-based platform to modulate fibronectin activity and focal adhesion assembly. Biores Open Access 3 (2014), 286-96.